Highly localized Wannier functions for the efficient modeling of Photonic Crystal Circuits

Matthias Schillinger[ab], Sergei F. Mingaleev[ac], Daniel Hermann[b], Kurt Busch[ab]

[a] Department of Physics and College of Optics & Photonics: CREOL & FPCE, University of Central Florida, Orlando, FL 32816, USA;
[b] Institut für Theorie der Kondensierten Materie, Universität Karlsruhe, 76128 Karlsruhe, Germany;
[c] Bogolyubov Institute for Theoretical Physics, 03143 Kiev, Ukraine

ABSTRACT

We present a novel approach for the accurate and efficient modeling of photonic crystal-based integrated optical circuits. Within this approach, the electromagnetic field is expanded into an orthogonal basis of highly localized Wannier functions, which reduces Maxwell's equations to *low-rank* eigenvalue problems (for defect mode and waveguide dispersion calculations) or to *sparse* systems of linear equations (for transmission/reflection calculations through/from functional elements). We illustrate the construction of Wannier functions as well as the subsequent determination of defect modes, waveguide dispersion relations, and the characterization of functional elements for realistic two-dimensional photonic crystal structures consisting of square and triangular lattices of air pores in a high-index matrix. Moreover, on the basis of our Wannier function calculations we suggest a novel type of broad-band integrated photonic crystal circuits based on the infiltration of low-index materials such as liquid crystals or polymers into individual pores of these systems. We illustrate this concept through the design of several functional elements such as bends, beam splitters, and waveguide crossings.

Keywords: Photonic Crystals, Devices, Wannier functions, Numerical methods, Integrated Optics

1. INTRODUCTION

Over the past years, substantial research efforts have been directed at investigations of Photonic Crystals (PCs) with embedded defects such as micro-cavities and waveguides. These structures hold tremendous potential for the creation of compact all-optical photonic integrated circuits. However, practical realizations of these expectations depend on optimized designs for integrated devices with complex functionalities. Despite the physical compactness of these envisaged devices, their modeling corresponds to numerically large problems so that all-purpose simulation techniques require formidable computational resources even for relatively simple devices. As a consequence, novel numerical methods for the efficient and accurate simulation of PC-based structures have to be developed. Ideally, these more specialized techniques may also provide additional insights into the physics of PCs and point to novel routes for approximate methods similar to the highly successful approximate methods of semiconductor physics.

In this manuscript, we present a highly efficient modeling approach which is based on the expansion of the electromagnetic field into an orthogonal set of localized photonic Wannier functions[1] which can be combined with a guided-mode scattering matrix approach[2] for maximum efficiency in the modeling of large-scale PC-based circuitry. We illustrate our approach for realistic two-dimensional (2D) PCs consisting of square and triangular lattices of air pores in a high-index matrix.

In Sec. 2, we provide a general discussion of Galerkin-type methods with a focus on a comparison of plane wave and Wannier function bases. In addition, we briefly illustrate the difficulties which arise in the construction of highly localized photonic Wannier functions and show how to overcome these problems with the help of recent developments in electronic structure theory.[3,4] In Sec. 3, we demonstrate the efficiency of the Wannier function approach by calculating localized defect modes and waveguiding modes that are created by infiltrating individual

Correspondence should be addressed to Kurt Busch: kbusch@physics.ucf.edu

Photonic Crystal Materials and Devices III, edited by Ali Adibi, Shawn-Yu Lin, Axel Scherer,
Proc. of SPIE Vol. 5733 (SPIE, Bellingham, WA, 2005) · 0277-786X/05/$15 · doi: 10.1117/12.591137

pores of 2D PCs with low-index materials such as liquid crystals or polymers. For E-polarized light, i.e. the electric field vector is directed parallel to the pore axis, this leads to essentially non-degenerate cavity modes and corresponding mono-moded waveguides which, in turn, suggest novel designs for devices. As an illustration of this concept, we present our designs for a set of functional elements that include waveguide bends, beam splitters, and waveguide crossings. These devices exhibit characteristics which are superior to devices based on missing pores and (owing to the tunability of the infiltrated material) are inherently tunable.[5]

2. GALERKIN TYPE METHODS FOR PHOTONIC CRYSTALS

In order to illustrate the Wannier function approach, we restrict ourselves to the case of the E-polarized light propagating in the (x, y)-plane of a 2D PC. In this case, for monochromatic light with frequency ω, i.e., $E(\mathbf{r}, t) = \exp(-i\omega t)E(\mathbf{r})$, Maxwell's equations reduce to a scalar wave equation for the z-component of the electric field

$$\nabla^2 E(\mathbf{r}) + \left(\frac{\omega}{c}\right)^2 \{\varepsilon_{\rm p}(\mathbf{r}) + \delta\varepsilon(\mathbf{r})\} E(\mathbf{r}) = 0 \; . \tag{1}$$

Here, c is the vacuum speed of light, $\mathbf{r} = (x, y)$ denotes the in-plane position vector, and $\nabla^2 = (\partial_x^2 + \partial_y^2)$ represents the 2D Laplacian. All the structural information of the PC is encoded into the dielectric function which we have decomposed into a spatially periodic part, $\varepsilon_{\rm p}(\mathbf{r})$, that describes the defect-free PC, and a contribution, $\delta\varepsilon(\mathbf{r})$, of the embedded defect structures. The wave equation (1) can be solved in many different ways. For example, it can be discretized in space and solved, e.g., with the numerical scattering matrix method.[6] However, these methods become inefficient for complex defect structures.

For many practically important problems more efficient approaches are those based on the expansion of the electric field into a complete set of orthogonal basis functions

$$E(\mathbf{r}) = \sum_\alpha E_\alpha \, \psi_\alpha(\mathbf{r}) \; , \tag{2}$$

where E_α is the amplitude associated with basis function $\psi_\alpha(\mathbf{r})$ and has to be determined through a matrix equation that is obtained by inserting this expansion into the wave equation (1)

$$\sum_\beta A_{\alpha\beta} \, E_\beta = \left(\frac{\omega}{c}\right)^2 \sum_\beta \{C_{\alpha\beta} + D_{\alpha\beta}\} \, E_\beta \; . \tag{3}$$

The matrices $\hat{A}$, $\hat{C}$, and $\hat{D}$ are defined as overlap integrals

$$A_{\alpha\beta} = -\int d^2\mathbf{r} \; \psi_\alpha^*(\mathbf{r}) \; \nabla^2 \; \psi_\beta(\mathbf{r}) \; , \tag{4}$$

$$C_{\alpha\beta} = \int d^2\mathbf{r} \; \psi_\alpha^*(\mathbf{r}) \; \varepsilon_p(\mathbf{r}) \; \psi_\beta(\mathbf{r}) \; , \tag{5}$$

$$D_{\alpha\beta} = \int d^2\mathbf{r} \; \psi_\alpha^*(\mathbf{r}) \; \delta\varepsilon(\mathbf{r}) \; \psi_\beta(\mathbf{r}) \; . \tag{6}$$

This so-called Galerkin approach reduces the problem of solving the *partial differential* equation (1) to the problem of solving an eigenvalue problem (for defect modes and waveguide dispersion relations) or a system of linear equations (for transmission/reflection calculations). The efficiency of this approach depends crucially on an appropriate choice of the set of basis functions for the problem at hand.

Plane Wave Basis

For the calculation of the photonic band structure of perfectly periodic PCs, i.e., when $\delta\varepsilon(\mathbf{r}) \equiv 0$ in Eq. (1), the simplest and the most commonly used basis functions are plane waves (PWs). In this case the solutions of Eq. (1) are the so-called Bloch modes, $E_{n\mathbf{k}}(\mathbf{r})$, which are labeled by a wave vector $\mathbf{k}$ within the first Brillouin zone (BZ) and a band index n. Explicitly, the Bloch-Floquet theorem states that

$$E_{n\mathbf{k}}(\mathbf{r}) = u_{n\mathbf{k}}(\mathbf{r}) \, e^{i\mathbf{k}\mathbf{r}} \; , \tag{7}$$

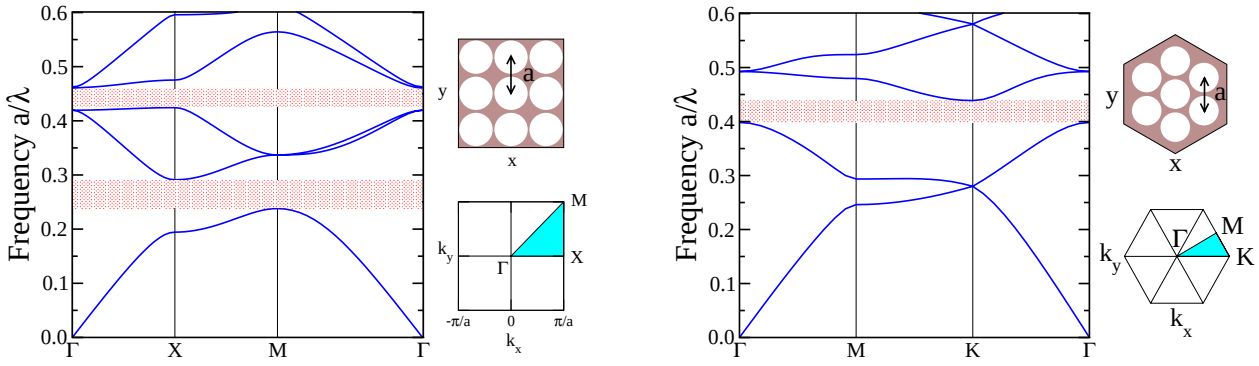

Figure 1. Photonic band structure for E-polarized light for two 2D macroporous silicon PCs. The upper insets show the underlying real space lattice (lattice constant a) of air pores (radius r) in silicon (dielectric constant $\varepsilon_b = 12$) for each system, whereas the lower ones depict the first BZ of the corresponding reciprocal lattice with their irreducible wedges highlighted. **Left panel:** Square lattice of air pores with $r/a = 0.475$. This PC exhibits two band gaps, with the fundamental band gap extending from $a/\lambda = 0.238$ to $a/\lambda = 0.291$ (20% of the midgap frequency). **Right panel:** Triangular lattice of air pores with $r/a = 0.45$. This PC exhibits a band gap between $a/\lambda = 0.398$ and $a/\lambda = 0.439$ (9.7% of the midgap frequency).

where the functions $u_{n\mathbf{k}}(\mathbf{r}) = u_{n\mathbf{k}}(\mathbf{r}+\mathbf{R})$ are periodic with respect to the set $\mathcal{R} = \{n_1\mathbf{a}_1 + n_2\mathbf{a}_2\,;\ (n_1, n_2)\ \in\ \mathcal{Z}^2\}$ of lattice vectors $\mathbf{R}$ that are generated by the primitive translations $\mathbf{a}_1$ and $\mathbf{a}_2$ that describe the periodicity of the dielectric function $\varepsilon_{\rm p}(\mathbf{r}+\mathbf{R}) = \varepsilon_{\rm p}(\mathbf{r})$. The eigenfrequencies, $\omega_{n\mathbf{k}}$, belonging to the Bloch functions, $E_{n\mathbf{k}}(\mathbf{r})$, acquire the same composite label $(n\mathbf{k})$ and may be represented in a photonic band structure diagram. As an example, we display in Fig. 1 the photonic band structure of the two model PCs which we will consider in the subsequent sections.

The periodic functions $u_{n\mathbf{k}}(\mathbf{r})$ can be expanded into plane waves, $e^{i\mathbf{G}_\alpha\mathbf{r}}$, where the vectors $\mathbf{G}_\alpha$ are the elements of the reciprocal lattice $\mathcal{G} = \{m_1\mathbf{b}_1 + m_2\mathbf{b}_2\,;\ (m_1, m_2)\ \in\ \mathcal{Z}^2\}$ whose primitive vectors $\mathbf{b}_1$ and $\mathbf{b}_2$ are defined by $\mathbf{b}_i\mathbf{a}_j = 2\pi\delta_{ij}$. Therefore, basis functions $\psi_\alpha(\mathbf{r}) \rightarrow e^{i(\mathbf{k}+\mathbf{G}_\alpha)\mathbf{r}}$ are appropriate expansion functions in Eq. (2) for each $E_{n\mathbf{k}}(\mathbf{r})$. In the case of 2D PCs consisting of *cylindrical* air pores of radius r in a high-index material with dielectric constant ε_b, we obtain

$$A_{\alpha\beta} = |\mathbf{k}+\mathbf{G}_\alpha|^2\delta_{\alpha\beta}\ \ , \qquad C_{\alpha\beta} = \varepsilon_b\delta_{\mathbf{G}_\alpha,\mathbf{G}_\beta} + 2\,f(r)\,(1-\varepsilon_b)\,\frac{J_1(|\mathbf{G}_\alpha - \mathbf{G}_\beta|r)}{|\mathbf{G}_\alpha - \mathbf{G}_\beta|r}\ , \tag{8}$$

where $f(r)$ is the pore filling fraction and $J_1(x)$ is the Bessel function of order one. Employing the asymptotics $J_1(x) \simeq \sqrt{2/\pi x}\cos(x - 3\pi/4)$ we obtain a slow power-law decay for the matrix elements $C_{\alpha\beta} \sim |\mathbf{G}_\alpha - \mathbf{G}_\beta|^{-3/2}$. This requires a relatively large number of plane waves (generally of about 1000) in order to obtain accurate results. In Fig. 1 we plot the photonic band structures for our two model PCs: a square lattice of air pores of radius $r = 0.475a$ and a triangular lattice of air pores of radius $r = 0.45a$ etched in silicon ($\varepsilon_b = 12$).[7]

Both model systems exhibit large photonic bandgaps so that through embedding defect structures described by non-zero $\delta\varepsilon(\mathbf{r})$ one can create localized defect modes with frequencies inside these band gaps. In principle, these modes can also be calculated with the plane waves approach by utilizing a super-cell approximation, i.e., periodically repeating $\delta\varepsilon(\mathbf{r})$ over a super-lattice with a sufficiently large super-cell period, N. However, in this case the required number of plane waves and, accordingly, the size of matrices $\hat{A}$, $\hat{C}$, and $\hat{D}$ grow as N^d, where $d = 2$ for 2D PCs considered here and $d = 3$ for 3D PCs. Therefore, the memory and CPU time requirements for standard eigenvalue algorithms grow roughly as N^{2d} and N^{3d}, respectively, and computational costs become over-excessive already for relatively small clusters of defects.

Wannier function basis

To reduce the size of matrices (4)–(6) for *localized* defect mode calculations, one can try to employ instead of *extended* plane waves certain *localized* basis functions, e.g., Hermite Gaussian functions.[8] This approach is more efficient than the PW method for calculations of simple defects.[8] However, for an extended cluster of defects or a PC circuit this, too, becomes over-excessive. The prime reason for this failure lies in the fact that special mathematical functions do not contain any information about the nature of the PCs unit cell, let alone of the underlying PC's photonic band structure. As a consequence a basis of all-purpose functions is never the optimal one, and therefore one practically always needs to use hundreds of these functions to accurately represent the electromagnetic field distributions of localized defect modes in any given PC.

Based on these considerations, it appears to be more reasonable to first create an optimal set of basis functions for a given underlying PC structure — the corresponding reduced load and speedup of defect mode and transmission calculations for optimized designs of functional elements will easily outweigh even fairly large computational costs in the creation of this basis. Specifically, an optimal basis should (i) consist of well-localized functions and (ii) contain all the information of the underlying photonic band structure. A corresponding set of basis functions are the so-called Wannier functions[9] defined through a lattice Fourier transform of the Bloch modes

$$W_{n\mathbf{R}}(\mathbf{r}) = \frac{V_{\mathrm{WSC}}}{(2\pi)^2} \int_{\mathrm{BZ}} d^2\mathbf{k}\, e^{-i\mathbf{k}\mathbf{R}}\, E_{n\mathbf{k}}(\mathbf{r}) \;, \tag{9}$$

where the integration is performed over the first BZ of the reciprocal lattice and V_{WSC} denotes the volume of the Wigner-Seitz cell (WSC). The above definition associates the photonic Wannier function $W_{n\mathbf{R}}(\mathbf{r})$ with the frequency range covered by band n, and centers it around the corresponding lattice site $\mathbf{R}$. In addition, the completeness and orthogonality of the Bloch functions directly translate into corresponding properties of the photonic Wannier functions

$$\int_{\mathbf{R}^2} d^2\mathbf{r}\; W^*_{n'\mathbf{R}'}(\mathbf{r})\, \varepsilon_{\mathrm{p}}(\mathbf{r})\, W_{n\mathbf{R}}(\mathbf{r}) = \delta_{n'n}\, \delta_{\mathbf{R}'\mathbf{R}} \;. \tag{10}$$

By construction, the Wannier functions contain all the relevant information of the underlying PC such as the lattice symmetry and the photonic band structure. Unfortunately, computing the Wannier functions directly from the output of photonic band structure programs via Eq. (9) leads to functions with poor localization properties and erratic behavior. These problems originate from an indeterminacy of the Bloch functions with respect to a phase factor $e^{\imath\phi_n(\mathbf{k})}$ which can be chosen arbitrarily for each wave vector $\mathbf{k}$ and band n. For the case of a group of N_{W} entangled bands there exists even a stronger indeterminacy which can be represented through a free unitary transformation $U_{mn}(\mathbf{k})$ between the Bloch functions with wave vector $\mathbf{k}$,

$$E_{n\mathbf{k}}(\mathbf{r}) \to \sum_{m=1}^{N_{\mathrm{W}}} U_{mn}(\mathbf{k})\, E_{m\mathbf{k}}(\mathbf{r}) \;, \tag{11}$$

which leaves the orthogonality relation (10) unchanged. Fixing the random part of the phases of the individual Bloch functions by, for instance, requiring them to be real-valued at the origin of the WSC constitutes a simple choice of the unitary transformation $U_{mn}(\mathbf{k})$ and removes the erratic behavior of the Wannier functions to a large extent. However, while being quite efficient for energetically isolated bands, this procedure fails to generate well localized functions for energetically entangled bands. A solution to this unfortunate situation is provided by recent advances in electronic structure theory. Souza, Marzari and Vanderbilt[3,4] have outlined an efficient scheme for the computation of maximally localized Wannier functions by determining numerically a set of unitary matrices $U_{mn}(\mathbf{k})$ that minimizes an appropriate spread functional. In view of the translational properties of the Wannier functions,

$$W_{n\mathbf{R}}(\mathbf{r}) = W_{n\mathbf{0}}(\mathbf{r} - \mathbf{R}) \;, \tag{12}$$

this functional reads

$$\Omega = \sum_{n=1}^{N_{\mathrm{W}}} \left[\langle n\mathbf{0}|\, r^2\, |n\mathbf{0}\rangle - \langle n\mathbf{0}|\, \mathbf{r}\, |n\mathbf{0}\rangle^2 \right] = \mathrm{Min} \;. \tag{13}$$

Here, we introduced a shorthand notation for matrix elements

$$\langle n'\mathbf{R}'|\, f(\mathbf{r})\, |n\mathbf{R}\rangle = \int_{\mathbf{R}^2} d^2\mathbf{r}\; W^*_{n'\mathbf{R}'}(\mathbf{r})\, f(\mathbf{r})\, \varepsilon_{\mathrm{p}}(\mathbf{r})\, W_{n\mathbf{R}}(\mathbf{r})\;, \tag{14}$$

for any function $f(\mathbf{r})$. It should be emphasized that since the unitary transformation (11) mixes the bands, the index n of the Wannier functions can no longer be referred to as a *band index*, and should be considered a label instead. Nevertheless, one may still refer to it as to the *band index* of generalized bands[16] obtained from Eq. (11). In Fig. 2 we depict an exemplary set of maximally localized Wannier functions for both model systems, which were generated by minimization of the spread functional (13). Obviously, these functions are strongly localized and nicely reflect the symmetry of the underlying lattice.

Using these maximally localized Wannier functions as the expansion basis in (2) where the collective index $\alpha \to \{n, \mathbf{R}\}$ represents now the set of Wannier functions for different lattice sites $\mathbf{R}$ and bands n, i.e. $\psi_\alpha(\mathbf{r}) \to W_{n\mathbf{R}}(\mathbf{r})$, the matrix elements defined in Eqs. (4) - (6) become

$$A^{n'n}_{\mathbf{R}'\mathbf{R}} = \frac{V_{\mathrm{WSC}}}{(2\pi)^2} \int_{\mathrm{BZ}} d^2\mathbf{k}\; e^{i\mathbf{k}(\mathbf{R}'-\mathbf{R})} \sum_m U^+_{n'm}(\mathbf{k}) \left(\frac{\omega_{m\mathbf{k}}}{c}\right)^2 U_{mn}(\mathbf{k}) \tag{15}$$

$$C^{n'n}_{\mathbf{R}'\mathbf{R}} = \delta_{n'n}\, \delta_{\mathbf{R}'\mathbf{R}} \tag{16}$$

$$D^{n'n}_{\mathbf{R}'\mathbf{R}} = \int_{\mathbf{R}^2} d^2\mathbf{r}\; W^*_{n'\mathbf{R}'}(\mathbf{r})\, \delta\varepsilon(\mathbf{r})\, W_{n\mathbf{R}}(\mathbf{r})\;. \tag{17}$$

At this point the power of the Wannier function approach becomes apparent. Due to the orthonormality relations of the Wannier functions, Eq. (10), the matrix $\hat{C}$ reduces to the unity matrix. Furthermore, the hermitian and positive definite matrix $\hat{A}$ depends solely on the photonic band structure $\omega_{n\mathbf{k}}$ and contains all the information about the perfectly periodic PC. Due to the smoothness of $\omega_{n\mathbf{k}}$ with respect to the wave vector $\mathbf{k}$, the exponential factor in Eq. (15) leads to a very rapid decay of the magnitude of matrix elements with increasing separation $|\mathbf{R}' - \mathbf{R}|$ between lattice sites, effectively making the matrix $\hat{A}$ sparse. Finally, the matrix $\hat{D}$ represents the perturbations of the periodicity mediated by the defect $\delta\varepsilon(\mathbf{r})$. As a consequence of the localization properties of both the Wannier functions and the defect dielectric function, the hermitian matrix $\hat{D}$ is sparse as well. Additionally, if the primitive cell of the underlying lattice obeys inversion symmetry with respect to its center, the Wannier functions can be chosen to be purely real,[3] in which case the matrices $\hat{A}$ and $\hat{D}$ even become real and symmetric.

It should be pointed out that instead of working with the electric field,[17,18] one may equally well construct photonic Wannier functions for the magnetic field, as demonstrated by Whittaker and Croucher.[10] The only difference in this approach is that the weighting function $\varepsilon_{\mathrm{p}}(\mathbf{r})$ enters neither the orthogonality relations (10) nor the construction of matrix elements according to Eq. (14). Instead, the matrix elements of matrix $\hat{D}$ involve the overlap of derivatives of the Wannier functions with the defect dielectric function $\delta\varepsilon(\mathbf{r})$.

3. RESULTS

After successfully constructing photonic Wannier functions, we proceed to the calculations of the optical properties of defect structures embedded in our two model PCs. The simplest defects consist of single-pore cavities and we determine their eigenfrequencies together with the individual contributions of each Wannier function to the corresponding defect modes. This allows us to further improve the efficiency of the Wannier function approach by restricting the number of Wannier functions to those that have significant contributions to cavity modes. Subsequent calculations of waveguide dispersion relations and transmission/reflection calculations for simple functional elements within the Wannier approach have been compared with the results of standard simulation techniques such as finite element, finite-difference time-domain, and multiple multipole techniques and excellent agreement has been found in all cases. We find that the infiltration of individual pores with low-index materials such as liquid crystals or polymers provides significant advantages for the realization of functional elements when compared to other strategies that rely on not-etched pores and/or pores of different radii. In particular, we

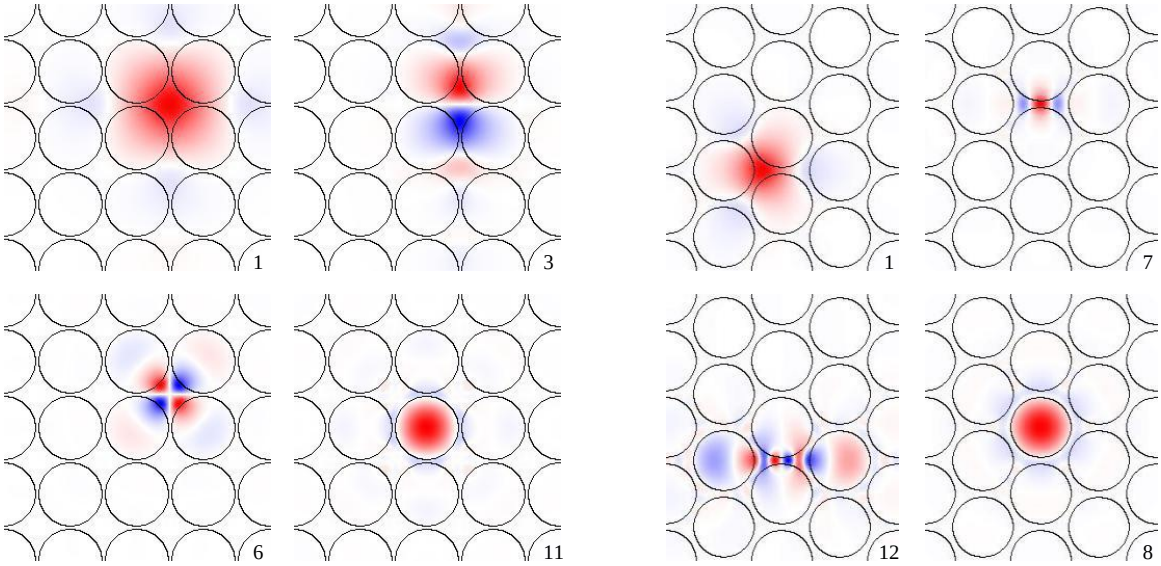

Figure 2. Maximally localized Wannier functions for (a) a square and (b) a triangular lattice of air pores etched into macroporous silicon. The generalized band index n is indicated in the lower right corners and the contribution of these functions to the defect mode is displayed in Fig. 3. The parameters and corresponding bandstructures of the underlying model systems are given in Fig. 1.

employ our Wannier function approach for obtaining novel designs of various functional elements which exploit the symmetry properties of localized cavity modes created by infilling a single pore with a low-index material. This novel concept allows us to achieve broad-band non-reflecting waveguide bends and beamsplitters as well as low-cross-talk intersections and tunable folded directional couplers.

3.1. Localized Cavity Modes

We start with studying simple cavities created by changing the dielectric constant $\varepsilon_{\rm def}$ of a single pore as shown in the insets of Figs. 3(a) and 3(b), respectively. For such a case the defect is described by

$$\delta\varepsilon(\mathbf{r}) = (\varepsilon_{\rm def} - \varepsilon_{\rm rod})\,\Theta(\mathbf{r} - \mathbf{R}_{\rm def})\;, \tag{18}$$

where $\Theta(\mathbf{r})$ defines the area of the defect pore. For a single infiltrated pore $\Theta(\mathbf{r}) = 1$ inside the pore at $\mathbf{R}_{\rm def} = \mathbf{0}$ and $\Theta(\mathbf{r}) = 0$ outside. In Figs. 3(a) and 3(b), we depict the dependence of the eigenfrequencies of the monopole-like cavity modes on the dielectric permittivity of the infilled material $\varepsilon_{\rm def}$ for our two model systems specified in Fig. 1. For both systems, a monopole-like defect mode emerges from the upper bandedge and traverses through the photonic band gap. Obviously the sensitivity of the defect frequency with respect to the refractive index is significantly higher for the triangular lattice than for the square lattice. Due to this higher sensitivity the triangular lattice may be preferable for the realization of tunable structures based on the low-index infiltration technique.

The symmetry properties of the cavity modes, which are shown in Figs. 4(b) and 4(d), clearly correlate with the symmetry of the underlying Wannier functions. This suggests that the convergence properties of the Wannier function approach depends on the nature and symmetry properties of the cavity modes under consideration. To determine the Wannier functions which provide the largest contribution to the defect mode, it is helpful to define a measure V_n of the strength of the contributions from the individual Wannier function associated with band n via

$$V_n = \sum_{\mathbf{R}} |E_{n\mathbf{R}}|^2\;. \tag{19}$$

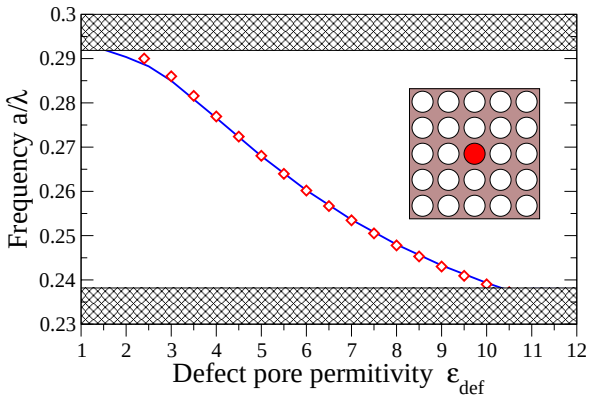

(a) Dependence of the defect frequency on ε_{def} for the square lattice system.

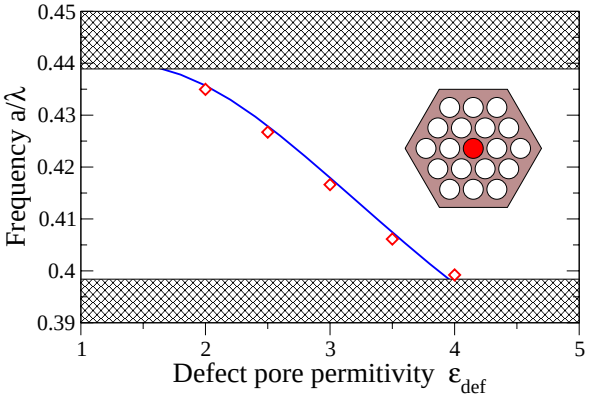

(b) Dependence of the defect frequency on ε_{def} for the triangular lattice system.

Figure 3. Frequencies of the localized defect modes associated with a single pore infilled with a material with dielectric constant ε_{def}. Values indicated with diamonds are calculated with our Wannier function approach by directly solving Eq. (3) as a generalized eigenvalue problem for the cavity frequencies that lie within the photonic band gap. The solid lines are calculated correspondingly using plane-wave-based super-cell calculations.[11] The parameters and corresponding bandstructures of the underlying model systems are given in Fig. 1.

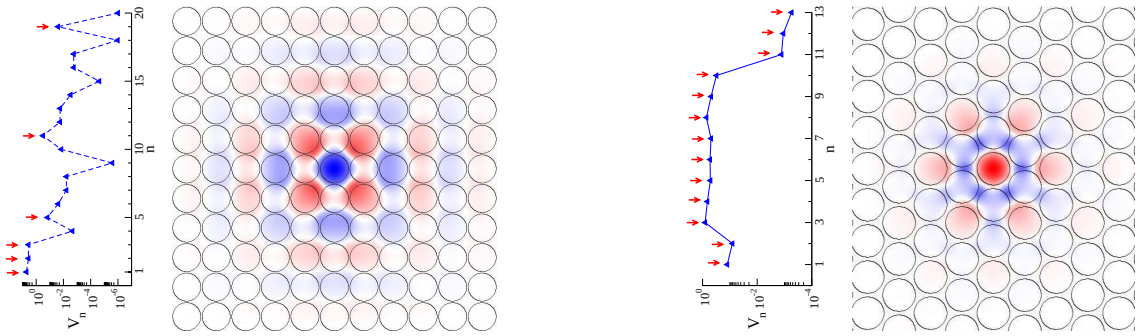

(a) (b) (c) (d)

Figure 4. Electric field distribution for the monopole-like cavity modes in a square lattice (b) and a triangular lattice (d) of air pores, which were created by infilling a single pore with a material of refractive index $\varepsilon_{\text{def}} = 2.40$ and $\varepsilon_{\text{def}} = 2.89$, respectively. (a) and (c) show the contribution of each single Wannier function, labeled with generalized index n, to the corresponding cavity mode measured with the parameter $V_n = \sum_R |E_{n\mathbf{R}}|^2$.

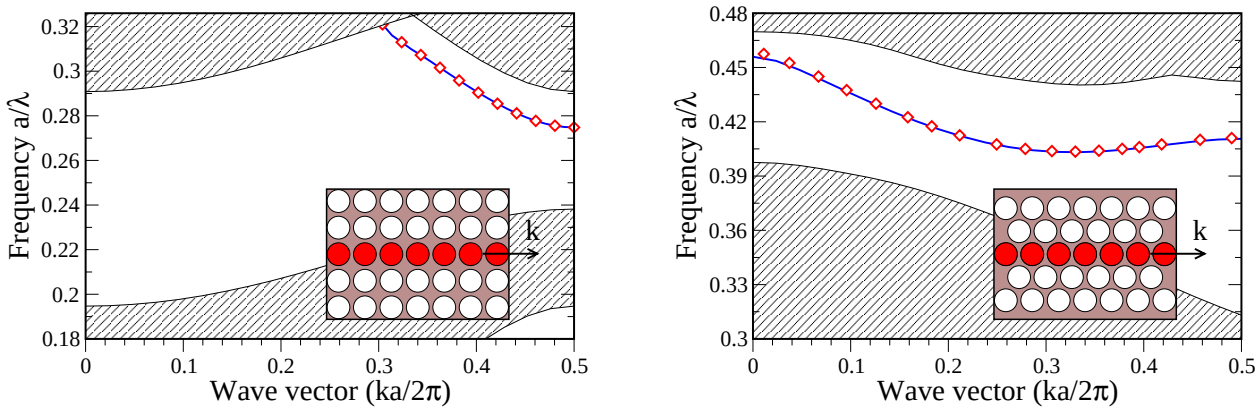

(a) Waveguide dispersion for the square lattice.

(b) Waveguide dispersion for the triangular lattice.

Figure 5. Dispersion relations for the propagating guided modes of waveguiding structures created by infiltration of a row of pores with materials specified in Fig. 4. The waveguide embedded into the square lattice is mono-moded throughout the complete passing band ranging from $a/\lambda = 0.275$ to $a/\lambda = 0.291$. Mono-moded operation for the waveguide created in the triangular lattice is possible for frequencies $a/\lambda = 0.410$ to $a/\lambda = 0.440$. The results obtained with the Wannier function approach, using $N_{\rm W} = 6$ and $N_{\rm W} = 13$ Wannier functions for the square lattice and the triangular lattice system, respectively, are indicated with diamonds and are in complete agreement with the results of plane-wave based supercell computations shown as solid line. The parameters and corresponding bandstructures of the underlying model systems are given in Fig. 1.

In Figs. 4(a) and 4(c), we display the dependence of the parameter V_n on the band index n for the cavity modes shown in Figs. 4(b) and 4(d), respectively. According to their contributions we choose a set of $N_{\rm W} = 6$ Wannier functions for the square lattice and $N_{\rm W} = 13$ for the triangular lattice system indicated with red arrows in Figs. 4(a) and 4(c) for the calculations described below.

3.2. Dispersion relations of Waveguides

Arguably the most important types of defect clusters in PCs are one or several adjacent straight rows of defects. Properly designed, such defect rows form a PC waveguide which allows the efficient guiding of light for frequencies within a photonic band gap.[13,14] Due to the one-dimensional periodicity of such a waveguide, its guided modes obey the 1D Bloch-Floquet theorem

$$E(\mathbf{r} + \mathbf{s}_{\rm w}) = e^{i\mathbf{k}(\omega)\mathbf{s}_{\rm w}}\, E(\mathbf{r}) \tag{20}$$

and thus they can be labeled by a wave vector, $\mathbf{k}(\omega)$, parallel to the waveguide director, $\mathbf{s}_{\rm w}{=}w_1\mathbf{a}_1 + w_2\mathbf{a}_2$, where $\mathbf{a}_1$ and $\mathbf{a}_2$ are the primitive lattice vectors of the PC, and integers w_1 and w_2 define the direction of the waveguide (for instance both W1-waveguides depicted in the insets of Fig. 5 can be described through $w_1{=}1$ and $w_2{=}0$ where $\mathbf{a}_1$ is pointing along the horizontal axis).

In Figs. 5(a) and 5(b) we present the dispersion relations of the propagating guided modes for the waveguides of our model systems (as indicated in the corresponding insets). The results obtained with our Wannier function approach are compared to calculations carried out by employing the supercell technique.[11,12]

At this point we would like to emphasize that, in contrast to the supercell technique, the Wannier function approach, enables us to also obtain the dispersion relations for *evanescent* guided modes, which obey Eq. (20) for complex wave vectors $\mathbf{k}(\omega)$ with non-zero imaginary part. Clearly, these modes are largely irrelevant in perfectly periodic straight waveguides. However, they do play an important role as soon as the perfect periodicity of the waveguide is broken either through imperfections due to fabrication tolerances, or through the deliberate creation of deviations from periodicity such as bends or coupled cavity-waveguide systems. In such cases, these *evanescent* guided modes give rise to light localization effects and determine the non-trivial transmission and

reflection properties of PC circuits. Furthermore, they allow for the calculation of the complex transmission and reflection amplitudes of multiport devices which will be presented below (see also Ref. 2).

3.3. PC Circuit Devices

Having established the basic properties of cavity modes and waveguides based on the infiltration of pores with low-index materials into our model PCs, we now present a set of functional elements for the creation of tunable PC circuits that combine several attractive advantages: (i) The PC circuits are based on 2D PCs consisting of air pores in high-refractive-index dielectrics and, therefore, can easily be fabricated. (ii) They exploit the *non-degenerate*, monopole-type defect modes for *E-polarized light* that result from infilling individual pores with appropriate low or moderate refractive index materials such as liquid crystals and/or polymers (see Fig. 4). By construction, this leads to *essentially mono-moded* PC waveguides. Furthermore, a peculiar symmetry of the square lattice cavity modes may be exploited to obtain designs for broad-band non-reflecting waveguide bends and beamsplitters as well as broad-band low-crosstalk waveguide intersections operating in *the same* frequency range. (iii) Owing to the tunability of the infilled materials the resulting circuits will be tunable.

The results for the transmission characteristics are obtained within the Wannier function approach by solving Eq. (3) in the basis of Wannier functions as a system of linear equations with the frequency as a given parameter. To this end, certain expansion coefficients $E_{n\mathbf{R}}$ are assigned values to specify an incoming waveguide mode, either propagating or evanescent. Of significant importance is the fact that, in contrast to most standard methods, the Wannier function approach permits the accurate and efficient calculation of the *complete scattering matrices* of PC devices which consist of complex scattering amplitudes connecting all, i.e., both propagating and evanescent, incoming with all outgoing channels and, therefore, contain all the phase relations and localization properties between these channels. As a consequence, it provides us with the possibility to model large-scale PC devices exploiting all the advantages of a guided-mode scattering matrix technique which is described in detail in Ref. 1 and Ref. 2, and is conceptually similar to the well-known cascaded impedance matrices of microwave theory.[20]

In Figs. 6 (a),(b),(d) we show several designs for waveguide bends with an angle of 90^o for the square lattice and angles of 60^o and 120^o for the triangular lattice PC. These bend designs exhibit excellent broad-band transmission characteristics. Based on the 90^o square lattice bend, we were also able to design a 90^o beamsplitter depicted in Fig. 6(c) with minimal reflection over the same broad frequency range as the bend. For the triangular lattice, however, he have not yet succeeded in finding a similarly efficient design for a beam splitter. Our preliminary investigation suggests that the localized defect mode for the triangular lattice obeys a higher rotational symmetry with respect to the vertical symmetry axis of the edged pores. As a result, the coupling between the waveguides in this simple design remains sub-optimal and more elaborate coupling elements need to be considered. Figs. 6(e) and 6(f) show waveguide intersections created for both model systems, where we have been able to almost completely eliminate parasitic cross-talk between the waveguides without having to take recourse to high-Q resonances as suggested in Ref. 19. As a result, our waveguide intersections operate over a reasonable broad range of frequencies.

Whereas the regions of high transmission significantly overlap for the devices embedded into the square lattice PC, the same does not hold for the devices in the triangular system. However, the triangular-lattice-based devices exhibit a roughly twice as large absolute bandwidth for each individual device. Therefore, a choice of the underlying lattice has to be made in a tradeoff between the requirements for absolute bandwidth of the planned PC circuit and the envisaged complexity that would combine several distinct functional elements.

We would like to emphasize that the designs discussed above are created out of physical intuition based on the symmetry of the underlying localized single cavity mode, which leads to several devices with nearly optimal transmission properties that - for the square lattice system - work in a common frequency band.

Further improvements of the above designs may be obtained by applying recently developed methods for PC-based device design optimization that utilize the full numerical efficiency of the Wannier function approach[15] together with the possibilities for fine tuning of device properties provided by the single pore infiltration technique through infilling different pores with materials of different refractive index.

Finally, we would like to demonstrate the tunability provided by the single pore infiltration technique by way of a folded directional coupler[21] (FDC) for the square lattice system which is depicted in Fig. 7(a). This

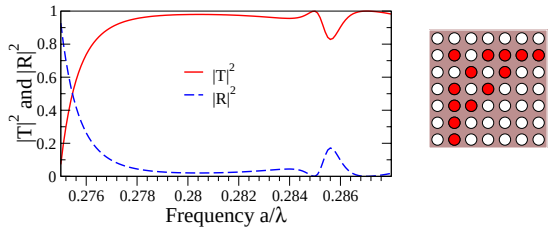

(a) 90^o waveguide bend for square lattice.

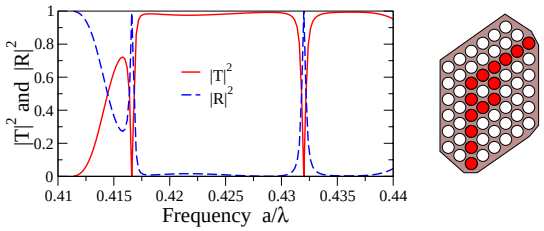

(b) 60^o waveguide bend for triangular lattice.

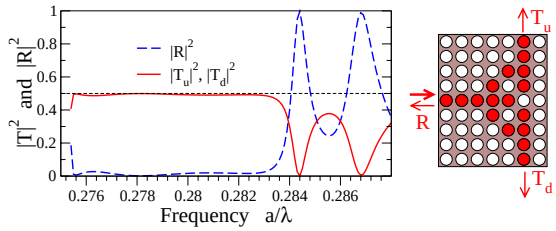

(c) 90^o beamsplitter for square lattice.

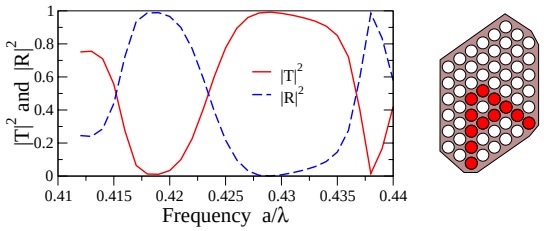

(d) 120^o waveguide bend for triangular lattice.

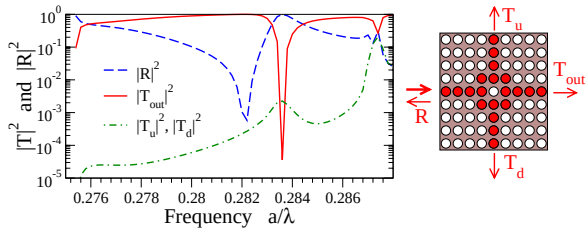

(e) Waveguide intersection square lattice.

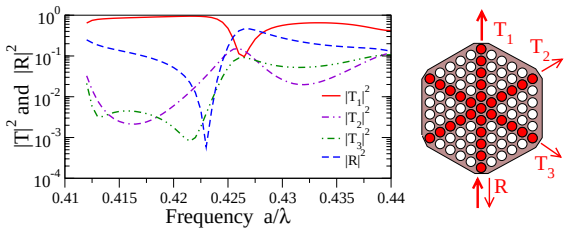

(f) Waveguide intersection triangular lattice.

Figure 6. Designs and transmission characteristics of different devices created by single pore infiltration with materials of dielectric permittivity $\varepsilon_{\text{def}} = 2.40$ for the square lattice and $\varepsilon_{\text{def}} = 2.89$ for the triangular lattice.

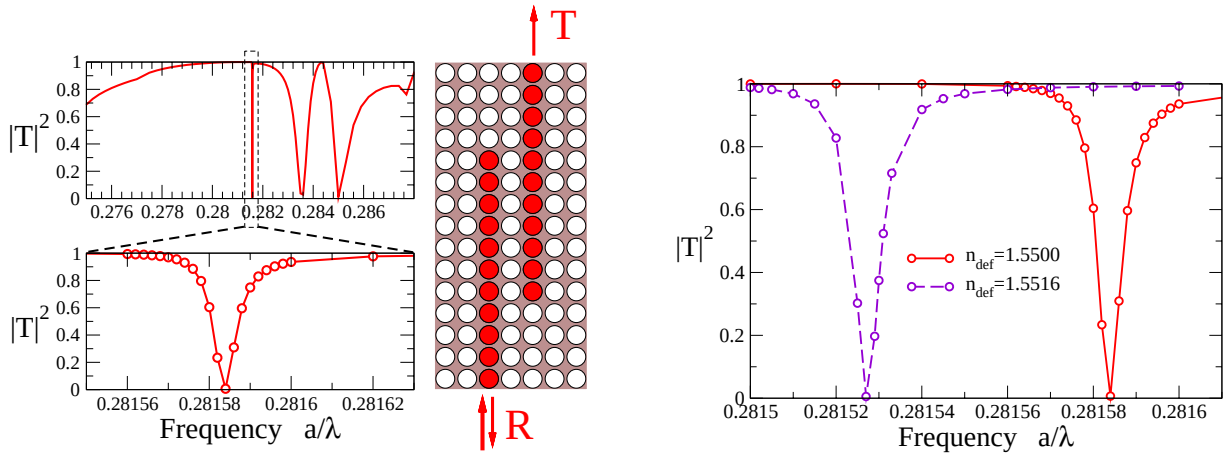

Figure 7. (a) Design and transmission spectrum for a folded directional coupler embedded into a square lattice of air pores. (b) Resonance dip of the transmission for different values of refractive index n of the infilled material. The parameters and corresponding bandstructures of the underlying model systems are given in Fig. 1.

FDC exhibits a sharp resonance with a quality factor $Q > 40,000$. Fig. 7(b) shows the change of the resonance frequency with respect to a change $\Delta n = 1.6 \cdot 10^{-3}$ of the refractive index. The resulting tunability may be expressed through the shift $\Delta\lambda/\lambda$ of the resonance wavelength. Our numerical results can be cast in form of a linear tuning in Δn: $\Delta\lambda/\lambda \approx 0.13\Delta n$. This tunability is solely based on the tunability of the infilled material. For instance, the birefringence of nematic liquid crystals can lead to values for Δn as large as 0.2, corresponding to rather substantial tuning ranges of the resonance frequency of the FDC.

4. ACKNOWLEDGMENTS

This work was in part supported by the Center for Functional Nanostructures (CFN) of the Deutsche Forschungsgemeinschaft (DFG) within projects A1.1 and A1.2. The work of M.S. is funded in parts through a one year PhD scholarship of the German Academic Exchange Service (DAAD) and within the framework of the DFG Research Training Group 786 *Mixed Fields and Nonlinear Interactions* at the University of Karlsruhe.

REFERENCES

1. K. Busch, S. F. Mingaleev, A. Garcia-Martin, M. Schillinger, and D. Hermann, "Wannier function approach to photonic crystal circuits", *J. Phys.: Condens. Matter.* **15**, pp. R1233–R1256, 2003.
2. S. F. Mingaleev and K. Busch, "Scattering matrix approach to large-scale photonic-crystal circuits", *Opt. Lett.* **28**, pp. 619–621, 2003.
3. N. Marzari and D. Vanderbilt, "Maximally localized generalized Wannier functions for composite energy bands", *Phys. Rev. B* **56**, pp. 12847–12865, 1997.
4. I. Souza, N. Marzari, and D. Vanderbilt, "Maximally localized Wannier functions for entangled energy bands", *Phys. Rev. B* **65**, pp. 035109–13, 2000.
5. S. F. Mingaleev, M. Schillinger, D. Hermann and K. Busch, "Tunable photonic crystal circuits: concepts and designs based on single-pore infiltration", *Opt. Lett.* **29**, pp. 2858–2860, 2004.
6. G. von Freymann, W. Koch, M. Wegener, M. Diem, A-M Garcia, Suresh Pereira, K. Busch, J. Schilling and R. Wehrspohn, "Diffraction properties of two-dimensional photonic crystals", *Appl. Phys. Lett.* **83**, pp. 614–616, 2003.

7. A. Birner, R. B. Wehrspohn, U. M. Gösele, and K. Busch, "Silicon-Based Photonic Crystals", *Adv. Mat.* **13**, pp. 377–388, 2001.
8. D. Mogilevtsev, T. A. Birks, and Ph. S. Russell, "Localized function method for modeling defect modes in 2-D photonic crystals", *J. Lightwave Technol.* **17**, pp. 2078–2081, 1999.
9. G. H. Wannier, "The structure of electronic excitation levels in insulating crystals", *Phys. Rev.* **52**, pp. 191–197, 1937.
10. D. M. Whittaker and M. P. Croucher, "Maximally localized Wannier functions for photonic lattices", *Phys. Rev. B* **67**, pp. 085204–6, 2003.
11. S. G. Johnson and J. D. Joannopoulos, "Block-iterative frequency-domain methods for Maxwell's equations in a planewave basis", *Opt. Express* **8**, pp. 173–190, 2001.
12. K. Busch and S. John, "Photonic band gap formation in certain self-organizing systems", *Phys. Rev. E* **58**, pp. 3896–3908, 1998.
13. A. Mekis, J. C. Chen, I. Kurland, S. H. Fan, P. R. Villeneuve, and J. D. Joannopoulos, "High transmission through sharp bends in photonic crystal waveguides", *Phys. Rev. Lett.* **77**, pp. 3787–3790, 1996.
14. J. D. Joannopoulos, P. R. Villeneuve, and S. H. Fan, "Photonic crystals: Putting a new twist on light", *Nature* **386**, pp. 143–149, 1997.
15. Y. Jiao, S. Fan, D. A. B. Miller, "Demonstration of systematic photonic crystal device design and optimization by low rank adjustments: an extremely compact mode separator", *Opt. Lett.* **30**, pp. 141–143, 2005.
16. W. Kohn, "Construction of Wannier functions and applications to energy bands", *Phys. Rev. B* **7**, pp. 4388–4398, 1973.
17. A. Garcia-Martin, D. Hermann, K. Busch, and P. Wölfle, "Solid state theoretical method for defect computations in photonic crystals", *Mat. Res. Soc. Symp. Proc.* **722**, pp. L1.1, 2002.
18. A. Garcia-Martin, D. Hermann, F. Hagmann, K. Busch, and P. Wölfle, "Defect computations in photonic crystals: A solid state theoretical approach", *Nanotechnology* **14**, pp. 177, 2003.
19. S. G. Johnson, C. Manolatou, S. H. Fan, P. R. Villeneuve, J. D. Joannopoulos, and H. A. Haus, "Elimination of cross talk in waveguide intersections", *Opt. Lett.* **23**, pp. 1855–1857, 1998.
20. H. Brand, *Schaltungslehre linearer Mikrowellennetze*, Hirzel, Stuttgart, 1970.
21. T. P. White, L. C. Botten, R. C. McPhedran, and C. M. de Sterke, "Ultracompact resonant filters in photonic crystals", *Opt. Lett.* **28**, pp. 2452–2454, 2003.